

# PCCP

Accepted Manuscript



This is an *Accepted Manuscript*, which has been through the Royal Society of Chemistry peer review process and has been accepted for publication.

*Accepted Manuscripts* are published online shortly after acceptance, before technical editing, formatting and proof reading. Using this free service, authors can make their results available to the community, in citable form, before we publish the edited article. We will replace this *Accepted Manuscript* with the edited and formatted *Advance Article* as soon as it is available.

You can find more information about *Accepted Manuscripts* in the [Information for Authors](#).

Please note that technical editing may introduce minor changes to the text and/or graphics, which may alter content. The journal's standard [Terms & Conditions](#) and the [Ethical guidelines](#) still apply. In no event shall the Royal Society of Chemistry be held responsible for any errors or omissions in this *Accepted Manuscript* or any consequences arising from the use of any information it contains.

## ARTICLE

## Sensitive fluorescence-based detection of magnetic field effects in photoreactions of flavins

Cite this: DOI: 10.1039/x0xx00000x

Emrys W. Evans,<sup>a</sup> Jing Li,<sup>b</sup> Jonathan G. Storey,<sup>a</sup> Kiminori Maeda,<sup>b,c</sup> Kevin B. Henbest,<sup>a</sup> P. J. Hore,<sup>b</sup> Stuart R. Mackenzie<sup>b\*</sup> and Christiane R. Timmel<sup>a\*</sup>Received 00th January 2012,  
Accepted 00th January 2012

DOI: 10.1039/x0xx00000x

www.rsc.org/

Magnetic field effect studies have been conducted on a variety of flavin-based radical pair systems chosen to model the magnetosensitivity of the photoinduced radical pairs found in cryptochrome flavoproteins. Cryptochromes are blue-light photoreceptor proteins which are thought to mediate avian magnetoreception, an hypothesis supported by recent *in vitro* observations of magnetic field-dependent reaction kinetics for a light-induced radical pair in a cryptochrome from the plant *Arabidopsis thaliana*. Many cryptochromes are difficult to express in large quantities or high concentrations and are easily photodegraded. Magnetic field effects are typically measured by spectroscopic detection of the transient radical (pair) concentrations. Due to its low sensitivity, single-pass transient absorption spectroscopy can be of limited use in such experiments and much recent work has involved development of other methodologies offering improved sensitivity. Here we explore the use of flavin fluorescence as the magnetosensitive probe and demonstrate the exceptional sensitivity of this technique which allows the detection of magnetic field effects in flavin samples at sub-nanomolar concentrations and in cryptochromes.

### Introduction

Magnetic field effects (MFEs) on flavin-based radical pair systems have been studied for many years.<sup>1</sup> This interest has intensified in the last decade following the proposal that cryptochrome, a blue-light photoreceptor protein, plays a key role in animal magnetoreception.<sup>2,3</sup> In these proteins, photoexcitation of the flavin adenine dinucleotide cofactor in its fully oxidized redox state, FAD, produces a singlet excited state, <sup>1</sup>FAD\*, which is then reduced on a picosecond timescale by consecutive electron transfers along a chain of three tryptophan (Trp) residues, generating the singlet radical pair, [<sup>1</sup>FAD<sup>•-</sup> Trp<sup>•+</sup>]. We have previously shown that in the case of cryptochrome from the plant *Arabidopsis thaliana* and the related *Escherichia coli* photolyase protein, this radical pair can then undergo magnetic field-dependent spin dynamics resulting in a magnetically sensitive concentration of radicals in the protein.<sup>4</sup> This was the first experimental evidence for a MFE on a cryptochrome *in vitro* but by no means provides conclusive proof for the identity of the magnetosensitive radical pair or indeed that the radical pair mechanism lies at the heart of animal magnetoreception<sup>5-7</sup>. For *in vitro* experiments, there are two major challenges at present: 1) the detection of effects in fields as weak as that of the Earth (~50  $\mu$ T) and 2) the detection of an anisotropic MFE (required for a magnetic compass). To address these questions experimentally, a significant

increase in detection sensitivity is required as both Earth-strength MFEs and anisotropic effects are likely to be small (< 1%) based on previous studies of *Arabidopsis thaliana* cryptochrome-1 (*AtCry1*) and a model chemical compass.<sup>4,8</sup>

Traditionally, MFEs on flavin-based systems have been measured using transient absorption spectroscopy.<sup>9-14</sup> Radical and/or ground state absorption in the presence and absence of an external magnetic field provides a direct probe of MFEs via the Beer-Lambert law. However, the flavoproteins of interest are typically available only in  $\mu$ M concentrations and  $\mu$ L volumes making single-pass absorption-based measurements challenging.

Such considerations motivated our development of optical cavity-based techniques for MFE detection in the forms of cavity ring-down spectroscopy (CRDS)<sup>15</sup> and broadband cavity-enhanced absorption spectroscopy (BBCEAS).<sup>16</sup> Both methods were shown to significantly improve the detection sensitivity whilst also minimising the extent of sample photodegradation.

If still higher sensitivity is required one alternative approach is to use fluorescence detection. To date, fluorescence-detected MFEs have largely been restricted to reactions that form luminescent products directly from the radical pair, a method that can be viewed as a 'delayed' fluorescence variant of the Magnetically Altered Reaction Yield (MARY) technique.<sup>17</sup> Examples of systems studied by delayed fluorescence MARY

include: photoexcited aromatic hydrocarbons (*e.g.* fluorene, anthracene, naphthalene) in hydrocarbon solvents (*e.g.* squalene, cyclohexane) that form magnetically sensitive, geminate radical ion pairs upon illumination and which recombine to fluorescent excited states,<sup>18-23</sup> and photoexcited pyrene and *N,N*-dimethylaniline solutions for which spin-selective recombination results in a fluorescent exciplex.<sup>17, 24, 25</sup> An alternative two-colour approach, in which a second excitation source excites fluorescence in a reaction product, has been used to study the photochemistry of anthraquinone in micellar solutions.<sup>26</sup>

Until now, flavin fluorescence has not been used in MFE studies but has seen widespread application in conformational studies,<sup>27</sup> for identifying the amino acid residues involved in electron transfer in flavoproteins,<sup>28, 29</sup> for the determination of rotational correlation times,<sup>30, 31</sup> and for imaging intracellular concentrations of flavin to study the energy metabolism of cells.<sup>32</sup> Here, we demonstrate a highly sensitive approach using flavin fluorescence to measure MFEs in intermolecular radical pair (RP) model systems and in a cryptochrome, *AtCry1*, a technique we refer to as 'prompt' fluorescence (PF) MARY.

## Experimental

### Chemical systems

All intermolecular flavin / donor model systems studied here are aqueous solutions containing either flavin mononucleotide (FMN) or riboflavin (RF) as the photosensitizer and electron acceptor together with a suitable electron donor, which may be tryptophan, either as the free amino acid or as an amino acid residue in the protein hen egg white lysozyme (HEWL), guanosine or the guanine and adenine bases in DNA.

Upon blue-light photoexcitation, the flavin, F, forms the fluorescent singlet excited state ( $^1F^*$ ) which undergoes rapid intersystem crossing on the timescale of a few nanoseconds to give the triplet excited state,<sup>33</sup> see figure 1. This triplet is susceptible to intermolecular electron transfer (ET) from a donor to produce, under conservation of total spin angular momentum, the triplet state geminate radical pair  $^3[F^{\bullet-} D^{\bullet+}]$ . Coherent interconversion to the singlet radical pair,  $^1[F^{\bullet-} D^{\bullet+}]$ , is driven by the magnetic hyperfine interactions between the electron spins and the surrounding magnetic nuclei ( $^1H$ ,  $^{14}N$ , *etc.*). An applied magnetic field with an intensity similar to or larger than the effective hyperfine coupling of the radical pair leads to a decrease in singlet-triplet mixing efficiency because two of the three triplet sublevels become energetically displaced from the singlet state. This in turn results in a decrease in the population of singlet radical pairs. Consequently, as geminate recombination can only occur from the singlet state (via reverse electron transfer, RET), there is a rise in the concentration of free radicals as the strength of the applied magnetic field is increased. Conventionally, it is the field-dependence of the radical pair concentration that is monitored experimentally, whereas here the MFE is detected via the flavin fluorescence. Flavin-derived radical pairs do not recombine to a fluorescent product so the delayed fluorescence MARY approach is not viable. Instead the continuous

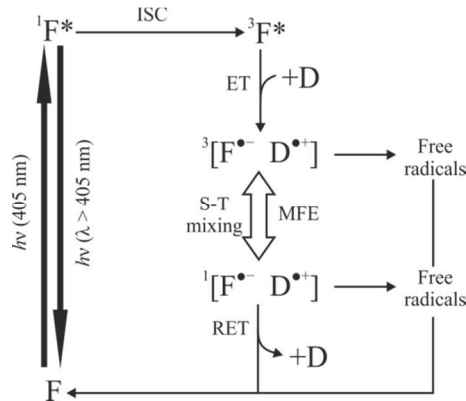


**Fig. 1:** Photochemical reaction scheme for the formation of intermolecular radical pairs involving a flavin (F) such as FMN or RF and an electron donor (D) such as Trp or guanosine. Following photoexcitation, the flavin excited state ( $^1F^*$ ) undergoes rapid intersystem crossing (ISC) to form the triplet state ( $^3F^*$ ), which is then susceptible to electron transfer (ET) resulting in the triplet-born spin-correlated radical pair. Magnetic field-dependent singlet-triplet mixing of the geminate radical pair influences its fate and is the origin of the magnetic field effects.

wave illumination experiment used here exploits the fluorescence of the excited photosensitizer itself.

FMN, RF, HEWL, tryptophan, guanosine monophosphate, DNA (from salmon testes, molecular weight =  $1.3 \times 10^6$  Da,  $\sim 2,000$  base pairs), and glycerol were purchased from Sigma Aldrich and used without further purification. All solutions were prepared using ultrapure water (Milli-Q).

*AtCry1* (full length cryptochrome-1) was provided by Planet Biotechnology, USA. The cryptochrome sample (50  $\mu M$ ) was studied in 50 mM Tris / HCl buffer at pH 7.0 with 100 mM NaCl and approximately 30% glycerol v/v.

### Apparatus

The experimental arrangement used for PF MARY is depicted in figure 2. Using a syringe pump (Chemyx, Fusion 100 Classic), solutions of the flavin / donor model systems were flowed at a rate of 0.25 mL  $\text{min}^{-1}$  through a sample cell (Starna Scientific, UV Quartz, 45/Q, 1 mm optical path length) so as to minimize photodegradation. The sample cell was positioned between a pair of Helmholtz coils which generated static magnetic fields of up to 14

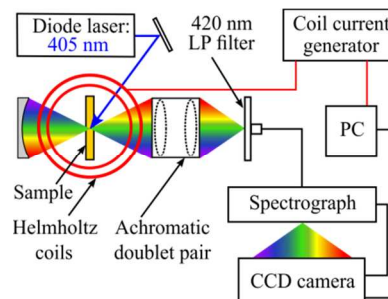


**Fig. 2:** Experimental arrangement used for PF MARY.

mT, reaching the desired value within 5 ms. A continuous wave diode laser (Power Technology, 405 nm, 350 mW) provided continuous photoexcitation of the sample and the response of the system's fluorescence was measured with the applied magnetic field switched alternately on and off. To ensure that the magnetic field had settled at the desired value, a delay of 50 ms was introduced between changing the field strength and detecting the fluorescence. The fluorescence was focussed using an achromatic doublet pair into an optical fibre coupled to a spectrograph (Andor Technology, SR-303i) which dispersed the light onto a charge-coupled device (CCD) camera (Andor Technology, Newton). The spectrograph slit width and camera exposure time (typically 20–60 ms) were optimized for each system studied to make full use of the dynamic range of the CCD detector. In some cases, to enable like for like comparisons under identical illumination conditions, it was necessary to attenuate the fluorescence itself with neutral density filters. The collection efficiency of the fluorescence was improved using a concave mirror at the rear of the optical cell and a 420 nm long-pass filter was employed to block the scattered light coming from the diode laser. All studies were conducted at room temperature (*ca.* 20°C) using integer field strengths between 0 and 14 mT, averaging 100–300 times at each field value in a random order. Each experiment took approximately 30 min.

Due to the limited availability of the cryptochrome sample, a miniaturized flow arrangement for studying the *AtCry1* system was necessary. This was achieved by employing a micropump (Bartels, mp6-pp) in association with a miniature flow cell (Hellma, Quartz SUPRASIL, 130.427 - QS). For the *AtCry1* studies a 450 nm diode laser was used for excitation to obtain a better match to the absorption profile; a 475 nm long-pass filter was employed to block scattered light. The laser output was attenuated to 1.7 mW so as to minimise photodegradation of the precious sample. This resulted in much reduced fluorescence and, in order to achieve good signal-to-noise, the signal integration times were increased to up to 5 s.

## Results and discussion

### Model systems

The photochemistry and magnetic sensitivity of the radical pair formed by photoexcitation of flavin/HEWL solutions have previously been characterized in some detail using absorption spectroscopy, making it an ideal candidate for proof-of-principle fluorescence detection studies.<sup>12, 15, 16, 34</sup>

Under the conditions employed here, the steady state concentrations of ground state F and F<sup>-</sup> (lifetime,  $\tau$  (F<sup>-</sup>)  $\approx$  10 ms)<sup>9, 12, 35-37</sup> greatly exceed those of the shorter lived <sup>1</sup>F\* ( $\tau$  = 19 ns), <sup>3</sup>F\* ( $\tau$   $\approx$  1–10  $\mu$ s),<sup>9, 12, 35-37</sup> and [F<sup>-</sup> D<sup>+</sup>] ( $\tau$   $\approx$  10 ns) species. It follows that:

$$[F]_{\text{total}} \approx [F] + [F^-]. \quad (1)$$

Thus, photostationary concentrations of F and F<sup>-</sup> are established, the relative amounts of which depend on the effective rate constants of free radical formation ( $\sim 10^3$  s<sup>-1</sup>) and decay ( $\sim 10^9$ – $10^{10}$  M<sup>-1</sup> s<sup>-1</sup>). A direct consequence of equation 1 is that any magnetic field-dependence of [F<sup>-</sup>] translates directly to an MFE on [F] and therefore on the fluorescence of <sup>1</sup>F\*. As the intensity of the magnetic field is increased and singlet-triplet interconversion becomes less efficient, fewer radical pairs recombine via the singlet radical pair state, and the concentration of free radicals rises. We therefore expect a reduction in the ground state concentration and therefore in the 'prompt' fluorescence from <sup>1</sup>F\*, *i.e.*, a negative MFE.

The red trace in figure 3 a) shows the fluorescence profile for 10  $\mu$ M FMN + 0.5 mM HEWL in aqueous solution in the absence of an applied magnetic field. The observed fluorescence spectral profile is in agreement with published spectra<sup>38</sup> and corresponds to the S<sub>1</sub>  $\rightarrow$  S<sub>0</sub> ( $\pi^* \rightarrow \pi$ ) transition of the FMN isoalloxazine moiety with a minor feature at 470 nm ascribed to the Raman scattering of the 405 nm laser light by water. As highlighted

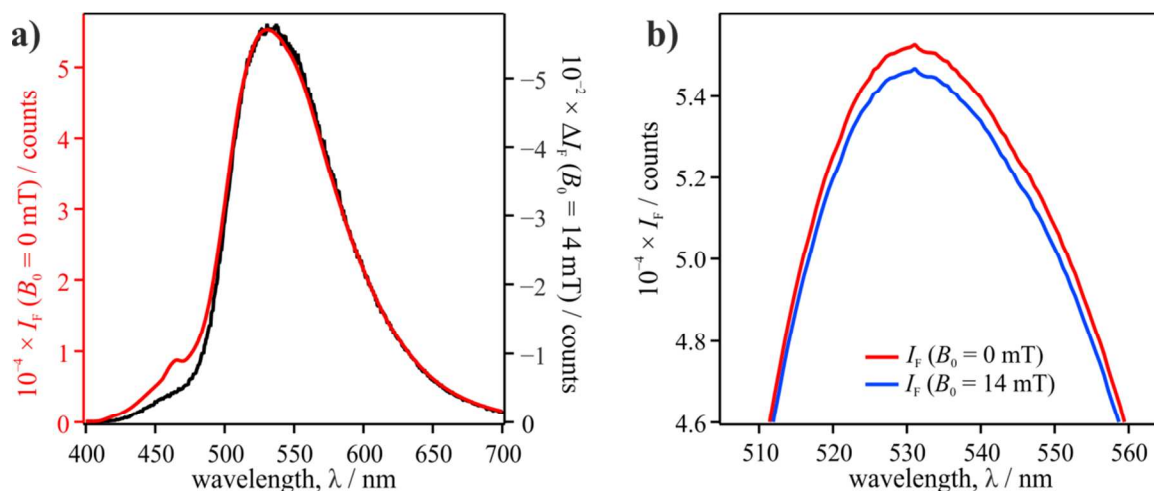


**Fig. 3:** a) Fluorescence intensity profile,  $I_f$ , for 10  $\mu$ M FMN + 0.5 mM HEWL in aqueous solution (red, left hand y-axis) in the absence of an applied magnetic field,  $B_0 = 0$  mT; and the fluorescence intensity subtraction profile (black, right hand y-axis),  $\Delta I_f$ , at magnetic field strength,  $B_0 = 14$  mT. b) Fluorescence intensity profiles obtained in the absence (red) and presence (blue) of a 14 mT magnetic field.

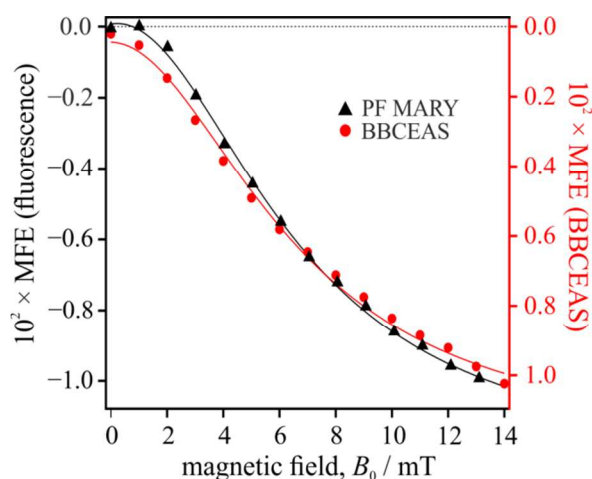


**Fig. 4:** MFE profiles for 10  $\mu\text{M}$  FMN + 0.5 mM HEWL in aqueous solution as obtained by BBCEAS (red circles) and PF MARY (black triangles). The lines are Lorentzian fits to the data.

in figure 3 b), a small decrease in fluorescence intensity is seen upon application of a  $B_0 = 14$  mT magnetic field (blue trace). The inverted difference between the two fluorescence profiles,  $\Delta I_F(B_0) = I_F(B_0) - I_F(0)$ , is shown as the black trace in figure 3 a). It coincides perfectly with the fluorescence profile of the FMN (apart from the Raman band). The negative MFE is reassuringly consistent with the radical pair mechanism for a triplet-born spin-correlated radical pair.

Formally, the MFE at magnetic field strength  $B_0$  is defined as:

$$\text{MFE}(B_0) = \Delta I_F(B_0) / I_F(0). \quad (2)$$

The PF MARY plot of  $\text{MFE}(B_0)$  for FMN/HEWL depicted in figure 4 (black triangles) has been averaged over the wavelength range 500–600 nm. It has a Lorentzian-like profile due to the expected

decrease in singlet-triplet mixing efficiency with increasing applied magnetic field strength. No inversion of the sign of the MFE is observed in weak magnetic fields (the so-called Low Field Effect<sup>39</sup>) in agreement with all previous studies of FMN/HEWL,<sup>12, 15, 16</sup> implying that the spin correlation in the radical pair relaxes (see below) before a weak applied field can affect the spin dynamics.

Also shown in figure 4 (red circles) is the MFE for the same system obtained by monitoring the radical absorption signal using BBCEAS.<sup>16</sup> The two curves have opposite signs (as expected from the two-state model in equation 1) and can be overlaid to highlight that both methods report on the magnetic sensitivity of the radical pair. Identical magnitudes for the MFEs measured by the two methods are not typically expected and, under these photoexcitation conditions, imply approximately equal populations of F and  $F^-$  (equation 1).

However, flavin photochemistry is more complex than shown in figure 1. Firstly, photodegradation of flavins leads to the production of lumichrome,<sup>40</sup> as confirmed by mass spectrometry (Fig. S1, Electronic Supplementary Information). Secondly, disproportionation of the neutral flavin radicals formed by protonation of  $F^-$  produces ground state flavin, F, and its fully reduced form,  $\text{FH}_2$ ,<sup>41</sup>



Both species thus inherit an MFE from the radicals. Lumichrome and  $\text{FH}_2$  are both detected in our experiments if the sample is not flowed (figure 5). The decrease in the sample absorbance between 400 and 500 nm as well as the increase in the fluorescence below  $\sim 475$  nm are consistent with the formation of lumichrome and/or fully reduced flavin. However, it is clear from figure 5 that the production of these species is much reduced when the solution is refreshed (by flowing, green dashed lines). As the data presented here were recorded exclusively using flowed samples, we may largely ignore these side reactions. Nevertheless, these processes are

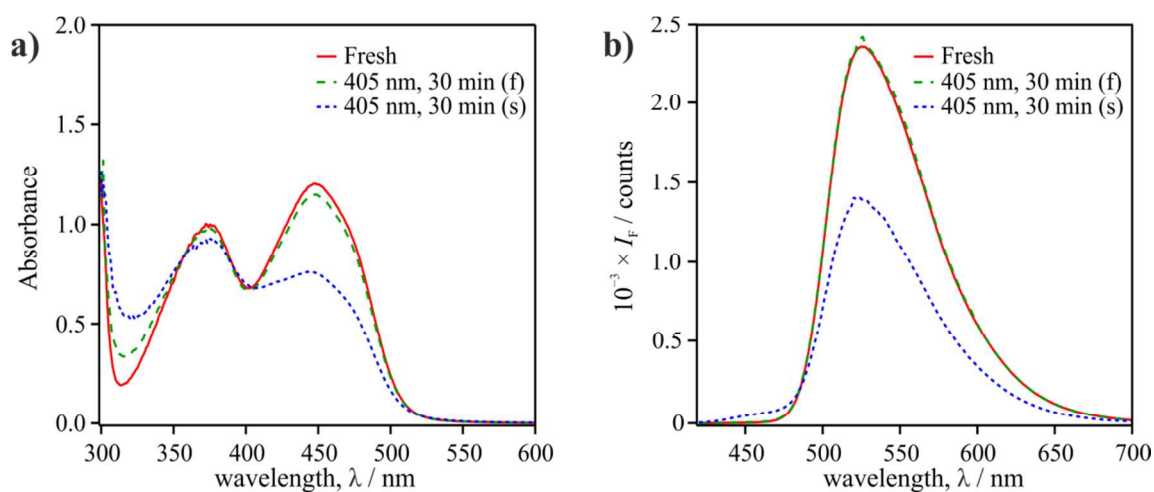


**Fig. 5:** a) UV/vis and b) fluorescence profiles of 100  $\mu\text{M}$  FMN + 0.5 mM HEWL in aqueous solution (solid red line, 'Fresh'). Following continuous photoexcitation by a 405 nm laser at 350 mW for 30 minutes, the spectra are virtually unaltered if the solution is continually refreshed as in the experiments conducted here (flow rate 0.5 mL  $\text{min}^{-1}$ , dashed green line) but significant changes are observed for a static sample (dotted blue line).

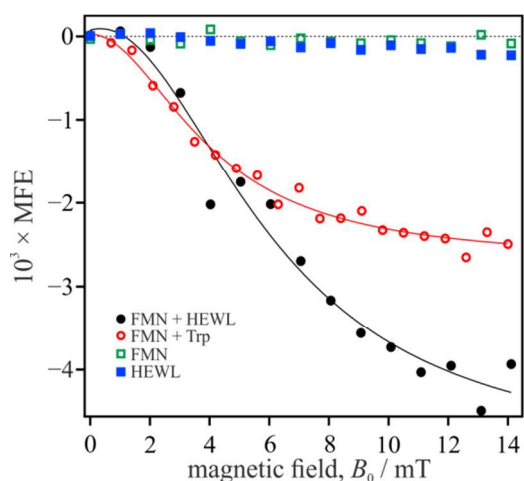


**Fig. 6:** PF MARY profiles: 1 nM FMN + 0.5 mM HEWL (filled black circles), 1 nM FMN + 0.5 mM Trp (open red circles), 1 nM FMN (open green squares) and 0.5 mM HEWL (filled blue squares), averaged over the wavelength range 500–600 nm. The red and black lines are Lorentzian fits to the data.

expected to impact the viability of the two-state model (equation 1) in determining flavin populations from MARY experiments obtained by prompt fluorescence and BBCEAS under identical photoexcitation conditions.

The sensitivity of the fluorescence-based MFE detection system is shown in figure 6 for a solution of 1 nM FMN + 0.5 mM HEWL (filled black circles) under the same illumination conditions as above. Shown in the same figure are data obtained for i) a solution of 1 nM FMN in the absence of electron donors (open green squares) and ii) a 0.5 mM solution of the protein alone (filled blue squares) as controls. An unambiguous MFE is detected with good signal-to-noise even under conditions that are beyond the sensitivity limits of our existing transient absorption and cavity-based absorption measurements.

MFEs for the FMN / HEWL reaction have a complex flavin concentration dependence arising from the detailed kinetics. A full discussion of these effects will be published elsewhere.

The final (open red circles) data in figure 6 depicts the PF MARY data obtained for a 1 nM solution of FMN in which the HEWL has been replaced by the amino acid tryptophan, Trp. Although an FMN-Trp radical pair is formed in both systems, a larger MFE at 14 mT is observed for the protein solution as the systems differ in their spin dynamics. This effect can be characterized by the empirical parameter,  $B_{1/2}$ , defining the magnetic field at which the MFE has reached half its maximum value, and typically obtained by Lorentzian fitting of the data. In the absence of spin relaxation,  $B_{1/2}$  is determined by the hyperfine couplings of the radical pair and, according to the Weller equation, equals 3.0 mT.<sup>4,42</sup> The larger experimental  $B_{1/2}$  values ( $3.5 \pm 0.1$  mT and  $6.5 \pm 0.1$  mT for the Trp and HEWL solutions, respectively) are consistent with previous findings and indicate the importance of spin relaxation in

both solutions.<sup>12, 15, 16</sup> The more pronounced effect for HEWL than Trp is probably caused by the slower relative diffusion of the components of the radical pair in the FMN/HEWL system. It is further enhanced by the Coulombic attraction of the negatively charged FMN and the positively charged protein (isoelectric point  $pI = 11.35$ ) which increases the lifetime of the radical pair during which dephasing processes begin to destroy the spin coherence leading, in turn, to broadening of the observed MARY profile.<sup>43,44</sup> It is instructive to compare the rotational correlation times ( $\tau_c$ ) of the larger, more slowly tumbling component in the two systems: (i) for FMN/Trp, the flavin has a rotational correlation time,  $\tau_c = 155$  ps,<sup>45</sup> (ii) for FMN/HEWL the protein tumbles much more slowly, with  $\tau_c = 7.2$  ns.<sup>46</sup> As shown in Refs<sup>43,44</sup>, in weak magnetic fields (*i.e.*,  $B_0 < 10 a_{\text{eff}}$ , where  $a_{\text{eff}}$  is the effective hyperfine coupling<sup>42</sup>), the slower the rotational motion, the more pronounced is the spin-dephasing and the greater is the deviation of the experimental  $B_{1/2}$  from that predicted by the Weller formula.

A similar effect on the shape of the PF MARY curve is observed for the radical pair formed by photoinduced electron transfer from guanosine to FMN, figure 7. The PF MARY curve broadens considerably when the free base guanosine ( $B_{1/2} = 3.0 \pm 0.1$  mT, blue) is replaced by DNA ( $B_{1/2} = 5.4 \pm 0.2$  mT, red). The DNA ( $\sim 1.3 \times 10^6$  Da) used in our studies is significantly larger than HEWL ( $1.42 \times 10^4$  Da). However, it is not possible to determine a unique rotational correlation time for DNA.<sup>47</sup> Different  $\tau_c$  values are obtained by NMR but all point to significantly faster motion than predicted by a rigid rod model of DNA. The NMR data provide evidence for considerable flexibility in certain structural features which are not exhibited by hydrodynamic measurements of DNA mobility.<sup>48</sup> A quantitative assessment of the relationship between the size of the DNA, its rotational correlation time and the observed broadening of the MARY data is thus not possible.

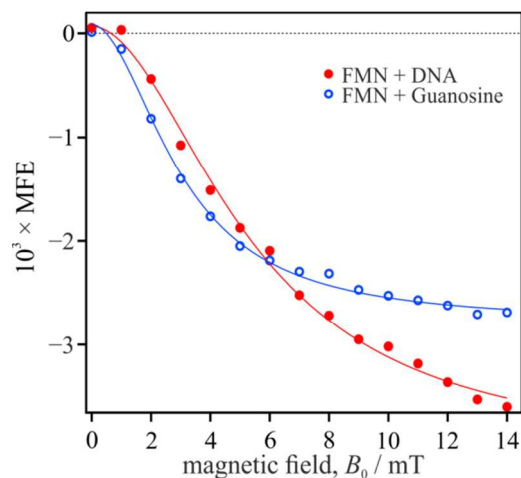


**Fig. 7:** PF MARY profiles: 10  $\mu$ M FMN + 10 mg mL<sup>-1</sup> ( $\sim 7.7$   $\mu$ M) DNA (filled red circles) and 10  $\mu$ M FMN + 1.0 mM guanosine (open blue circles), averaged over the wavelength range 500–600 nm. The lines are Lorentzian fits to the data.

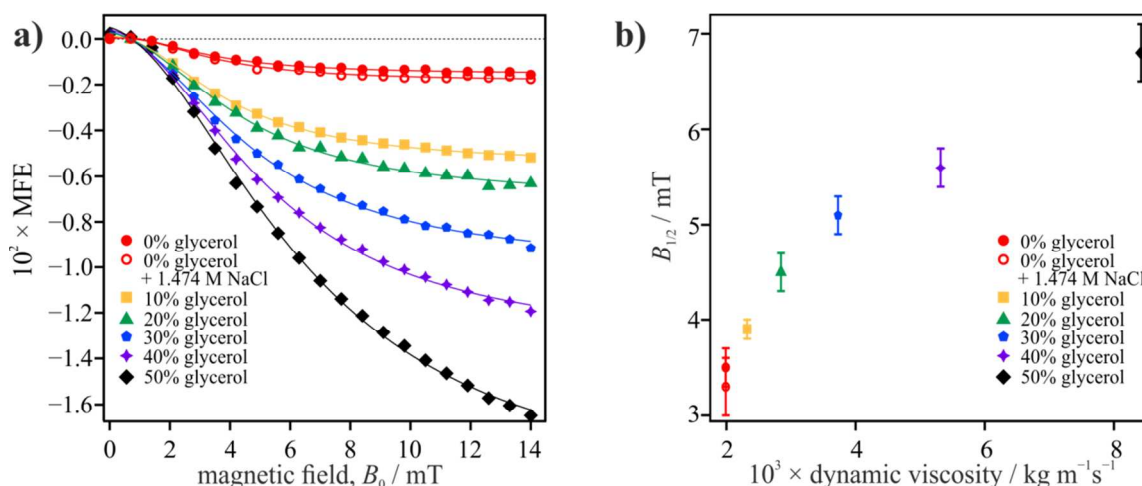


**Fig. 8:** a) PF MARY profiles (averaged over the wavelength range 500–600 nm) for 10 μM FMN and 0.5 mM Trp in aqueous solutions with different glycerol content (0–50% by volume). The lines are Lorentzian fits to the data and the resultant  $B_{1/2}$  values are plotted as a function of solvent viscosity in b).

The high quality of the present data does, however, allow a more systematic investigation of the relationship between  $B_{1/2}$  and  $\tau_c$  as a function of solvent viscosity using the Stokes relation:

$$\tau_c = \frac{4\pi\eta r_H^3}{3k_B T}, \quad (4)$$

in which  $\eta$  is the solvent viscosity and  $r_H$  is the hydrodynamic radius of the radical. Figure 8 a) shows PF MARY profiles for 10 μM FMN + 0.5 mM Trp in aqueous solutions of varying glycerol content. Figure 8 b) shows the measured  $B_{1/2}$  values as a function of solvent viscosity. A clear monotonic dependence of the MFE on  $B_0$  is observed for all viscosities consistent with dephasing being the cause of the increase in  $B_{1/2}$  with increasing glycerol concentration rather

than a combination of the hyperfine and conventional relaxation mechanisms. The latter would lead to an increased MFE at weak fields followed by a gradual increase at higher fields.<sup>43</sup> Maeda *et al.* have previously suggested that the effective relaxation rate between the singlet and triplet sublevels depends roughly linearly on the solution viscosity (see Ref<sup>44</sup> and equation 4 above):

$$k_{\text{relax}}^{\text{eff}} = \frac{0.5a_{\text{eff}}^2 T_2}{1 + (\omega_e T_2)^2} \approx \frac{0.5a_{\text{eff}}^2}{\omega_e^2 T_2} \approx A\tau_c \approx B\eta, \quad (5)$$

where  $\omega_e$  is the electron Zeeman frequency,  $T_2$  is the (dephasing) spin-spin relaxation time,  $A$  and  $B$  are constants for a given radical pair system, and  $1/T_2 \propto \tau_c$  is assumed. A simple relationship between the empirical parameter  $B_{1/2}$  and the solvent viscosity is neither expected nor observed. However, the data do confirm that dephasing becomes ever more significant as increased solvent viscosity restricts the motion of the radicals and prolongs the radical pair lifetime.

Increasing the glycerol fraction also changes the dielectric constant (relative permittivity) of the solution. However, this is expected to have little or no effect on the MFE of the FMN/Trp solution because, at pH 7.7, the tryptophan radical exists in its neutral form ( $\text{p}K_a(\text{Trp}^+) = 4.5$ ) so that there is no Coulombic attraction between the RP components. The open red circles in figure 8 show the PF MARY data obtained for a glycerol-free sodium chloride solution with the same dielectric constant as the 50% glycerol solution without NaCl (filled black diamonds). The increase in viscosity is clearly the dominant factor in broadening the MARY data. Moreover, the size of the observed MFE also grows with solvent viscosity as expected when radical recombination is slowed down in the more viscous solution.

Finally, the effects of changing the dielectric constant and viscosity of the solvent have been investigated for a number of flavin/HEWL systems and the results are shown in figure 9. As previously shown by Maeda *et al.*,<sup>12</sup> the addition of salt (NaCl) screens the Coulombic attraction between the FMN<sup>•-</sup> radical and the

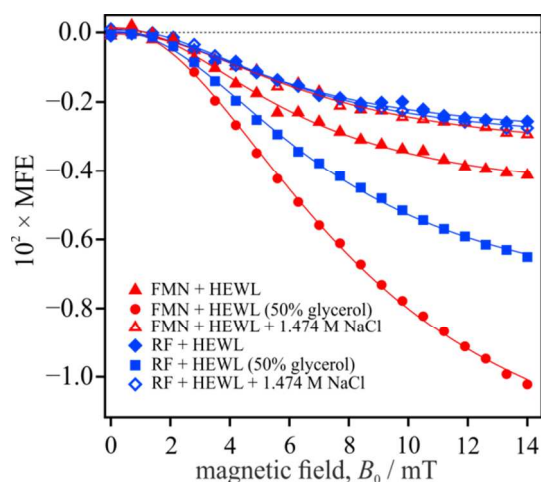


**Fig. 9:** PF MARY profiles for 10 μM FMN + 0.2 mM HEWL and 10 μM RF + 0.2 mM HEWL in aqueous solutions with varying NaCl concentration and glycerol content (% by volume), averaged over the wavelength range 500–600 nm. The lines are Lorentzian fits to the data.

positively charged HEWL resulting in a shorter lifetime of the radical pair and a concomitant decrease in both the MFE and  $B_{1/2}$ . Similar viscosity effects as described for the FMN/Trp solutions above are also observed.

The dependence of the MFE on changing glycerol and salt concentrations has also been investigated in a solution of riboflavin and HEWL (figure 9). RF and FMN are photochemically similar due to their common isoalloxazine group. However, RF does not have a charged phosphate group and thus has a reduced Coulombic attraction to HEWL. Hence, the RF/HEWL PF MARY profile exhibits no salt dependence but does show a growth in  $B_{1/2}$  with increasing solvent viscosity, as observed for the other flavin reactions investigated here.

### Cryptochrome

Blue light photoexcitation of the flavin (FAD) moiety in cryptochrome proteins triggers intramolecular electron transfer along a triad of tryptophan residues resulting in the formation of a singlet-born FAD-Trp radical pair. This behaviour contrasts with that of the HEWL/FMN model system which forms a triplet radical pair via intermolecular electron transfer. Consequently, an applied magnetic field has the opposite effect in the two systems: a large magnetic field which hinders singlet-triplet mixing leads to an *increase* in the flavin fluorescence for singlet-born radical pairs in cryptochrome (a positive MFE) in the same way that it decreases the fluorescence in the triplet-born (HEWL/FMN) system.

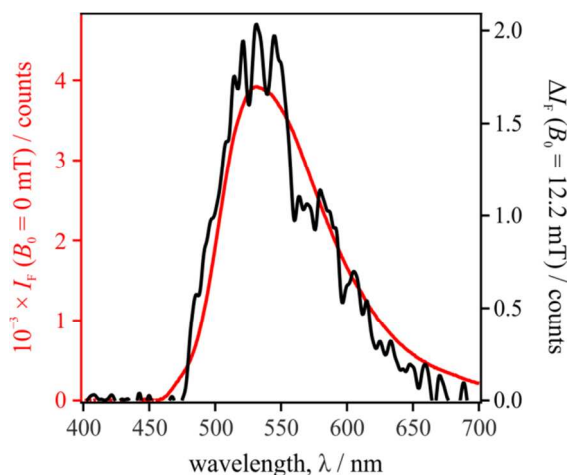


**Fig. 10:** A magnetic field effect in *AtCryI* detected by prompt fluorescence. Fluorescence intensity profile,  $I_F$ , for 50  $\mu$ M *AtCryI* in 50 mM Tris/HCl + 100 mM NaCl buffer, pH 7.0, glycerol 30% v/v (red, left hand y-axis) in the absence of an applied magnetic field,  $B_0 = 0$  mT; and the fluorescence intensity subtraction profile (black, right hand y-axis),  $\Delta I_F$ , at magnetic field strength,  $B_0 = 12.2$  mT.

Figure 10 shows the fluorescence profile and an unambiguous, positive MFE in *AtCryI* recorded via prompt fluorescence at a field of 12.2 mT. Gentle photoexcitation (450 nm at 1.7 mW) and low temperature (4°C) conditions were employed in an attempt to minimize sample degradation. From the scaled spectral profiles for both  $I_F(B_0 = 0$  mT) and  $\Delta I_F(B_0 =$

12.2 mT), we conclude that the magnetic field-dependent fluorescence is derived from the oxidized form of the flavin<sup>49</sup>. The band-averaged (500-600 nm) MFE is  $0.034\% \pm 0.007\%$  (1 standard error). The detected MFE is very small but statistically significant (see Electronic Supplementary Information for hypothesis testing). The small MFE compared to intermolecular flavin / donor systems is attributed to the similar reactivity of the singlet and triplet radical pairs in the protein. Nevertheless, this result clearly demonstrates the potential of this new approach to MFE-detection for studying biologically-relevant systems such as cryptochromes.

### Conclusions

A novel detection scheme for investigating MFEs in flavin-based systems has been developed. Its exceptional sensitivity enables field effects to be detected for samples containing as little as 1 nM flavin as well as for cryptochromes. This technique involves monitoring magnetic field-dependent changes in the prompt fluorescence of a continuously photoexcited system, which is shown to reflect the magnetosensitivity of the radical pair. The high sensitivity of this approach is used in characterizing the influence of external factors on the spin dynamics of the geminate pair and the size of the MFE in intermolecular reactions of flavins. Finally, we have succeeded in applying this detection method to measure a magnetic field effect in a cryptochrome. With continued optimisation we believe this method is ideally suited for studying intramolecular radical pairs in the flavoproteins that have been proposed as compass magnetoreceptors.

### Acknowledgements

This work was supported by the Defence Advanced Research Projects Agency (QuBE: N66001-10-1-4061), the European Research Council (under the European Union's 7th Framework Programme, FP7/2007-2013/ERC grant agreement no. 340451), the Air Force Office of Scientific Research (Air Force Materiel Command, USAF award no. FA9550-14-1-0095), the EMF Biological Research Trust, and JSPS KAKENHI Grant-in-Aid for Scientific Research (grant no. 26888004).

### Notes and references

<sup>a</sup>Department of Chemistry, University of Oxford, Inorganic Chemistry Laboratory, Oxford, OX1 3QR, UK.

<sup>b</sup>Department of Chemistry, University of Oxford, Physical & Theoretical Chemistry Laboratory, Oxford, OX1 3QZ, UK.

<sup>c</sup>Current address: Graduate School of Science and Engineering, Saitama University, 255 Shimo-Okubo, Sakura-ku, Saitama City, Saitama 338-8570, Japan.

<sup>d</sup>Both of these authors contributed equally to this work.

\*Correspondence may be addressed to:

stuart.mackenzie@chem.ox.ac.uk or

christiane.timmel@chem.ox.ac.uk.

Electronic Supplementary Information (ESI) available: Analysis of flavin photoproducts by mass spectrometry and hypothesis testing for *AtCry1* MFE. See DOI: 10.1039/b000000x/

1. R. Kaptein, K. Dijkstra and K. Nicolay, *Nature*, 1978, **274**, 293-294.
2. M. Ahmad and A. R. Cashmore, *Nature*, 1993, **366**, 162-166.
3. T. Ritz, S. Adem and K. Schulten, *Biophys. J.*, 2000, **78**, 707-718.
4. K. Maeda, A. J. Robinson, K. B. Henbest, H. J. Hogben, T. Biskup, M. Ahmad, E. Schleicher, S. Weber, C. R. Timmel and P. J. Hore, *Proc. Natl. Acad. Sci. USA*, 2012, 4774-4779.
5. C. Niessner, S. Denzau, K. Stapput, M. Ahmad, L. Peichl, W. Wiltshcko and R. Wiltshcko, *J R Soc Interface*, 2013, **10**, 20130638.
6. A. A. Lee, J. C. S. Lau, H. J. Hogben, T. Biskup, D. R. Kattinig and P. J. Hore, *J R Soc Interface*, 2014, **11**, 20131063.
7. H. J. Hogben, T. Biskup and P. J. Hore, *Phys Rev Lett*, 2012, **109**, 220501.
8. K. Maeda, K. B. Henbest, F. Cintolesi, I. Kuprov, C. T. Rodgers, P. A. Liddell, D. Gust, C. R. Timmel and P. J. Hore, *Nature*, 2008, **453**, 387-390.
9. Y. P. Tsentelovich, J. J. Lopez, P. J. Hore and R. Z. Sagdeev, *Spectrochim. Acta A*, 2002, **58**, 2043-2050.
10. M. Murakami, K. Maeda and T. Arai, *Chem. Phys. Lett.*, 2002, **362**, 123-129.
11. M. Horiuchi, K. Maeda and T. Arai, *App. Magn. Reson.*, 2003, **23**, 309-318.
12. T. Miura, K. Maeda and T. Arai, *J. Phys. Chem. B*, 2003, **107**, 6474-6478.
13. M. Horiuchi, K. Maeda and T. Arai, *Chem. Phys. Lett.*, 2004, **394**, 344-348.
14. M. Murakami, K. Maeda and T. Arai, *J. Phys. Chem. A*, 2005, **109**, 5793-5800.
15. K. Maeda, S. R. T. Neil, K. B. Henbest, S. Weber, E. Schleicher, P. J. Hore, S. R. Mackenzie and C. R. Timmel, *J. Am. Chem. Soc.*, 2011, **133**, 17807-17815.
16. S. R. T. Neil, J. Li, D. M. W. Sheppard, J. Storey, K. Maeda, K. B. Henbest, P. J. Hore, C. R. Timmel and S. R. Mackenzie, *J. Phys. Chem. B*, 2014, **118**, 4177-4184.
17. K. Schulten, H. Staerk, A. Weller, H. J. Werner and B. Nickel, *Z. Physik. Chem. NF*, 1976, **101**, 371-390.
18. B. Brocklehurst, R. S. Dixon, E. M. Gardy, V. J. Lopata, M. J. Quinn, A. Singh and F. P. Sargent, *Chem. Phys. Lett.*, 1974, **28**, 361-363.
19. R. S. Dixon, E. M. Gardy, V. J. Lopata and F. P. Sargent, *Chem. Phys. Lett.*, 1975, **30**, 463-464.
20. F. P. Sargent, B. Brocklehurst, R. S. Dixon, E. M. Gardy, V. J. Lopata and A. Singh, *J. Phys. Chem.*, 1977, **81**, 815-819.
21. R. S. Dixon, F. P. Sargent, V. J. Lopata, E. M. Gardy and B. Brocklehurst, *Can. J. Chem.*, 1977, **55**, 2093-2101.
22. R. S. Dixon, F. P. Sargent, V. J. Lopata and E. M. Gardy, *Chem. Phys. Lett.*, 1977, **47**, 108-112.
23. R. S. Dixon and V. J. Lopata, *Can. J. Chem.*, 1979, **57**, 3023-3027.
24. A. Weller, *Z. Physik. Chem. NF*, 1982, **130**, 129-138.
25. H. Staerk, W. Kuhnle, R. Treichel and A. Weller, *Chem. Phys. Lett.*, 1985, **118**, 19-24.
26. Y. Tanimoto, K. Shimizu and M. Itoh, *Chem. Phys. Lett.*, 1984, **112**, 217-219.
27. A. J. W. G. Visser, *Photochem. Photobiol.*, 1984, **40**, 703-706.
28. P. A. W. van den Berg, A. van Hoek, C. D. Walentas, R. N. Perham and A. J. W. G. Visser, *Biophys. J.*, 1998, **74**, 2046-2058.
29. H. Yang, G. Luo, P. Karnchanaphanurach, T.-M. Louie, I. Rech, S. Cova, L. Xun and X. S. Xie, *Science*, 2003, **302**, 262-266.
30. R. Leenders, A. Van Hoek, M. Van Iersel, C. Veeger and A. J. W. G. Visser, *Eur. J. Biochem.*, 1993, **218**, 977-984.
31. P. A. W. van den Berg, A. van Hoek and A. J. W. G. Visser, *Biophys. J.*, 2004, **87**, 2577-2586.
32. S. Huang, A. A. Heikal and W. W. Webb, *Biophys. J.*, 2002, **82**, 2811-2825.
33. S. D. M. Islam, A. Penzkofer and P. Hegemann, *Chem. Phys.*, 2003, **291**, 97-114.
34. E. W. Evans, C. A. Dodson, K. Maeda, T. Biskup, C. J. Wedge and C. R. Timmel, *J. R. Soc. Interface Focus*, 2013, **3**, 20130037.
35. D. B. McCormick, *Photochem. Photobiol.*, 1977, **26**, 169-182.
36. P. F. Heelis, B. J. Parsons, G. O. Phillips and J. F. McKellar, *Photochem. Photobiol.*, 1978, **28**, 169-173.
37. P. F. Heelis, B. J. Parson and G. O. Phillips, *Biochim. Biophys. Acta*, 1979, **587**, 455-462.
38. A. Bowd, P. Byrom, J. B. Hudson and J. H. Turnbull, *Photochem. Photobiol.*, 1968, **8**, 1-10.
39. C. R. Timmel, U. Till, B. Brocklehurst, K. A. McLauchlan and P. J. Hore, *Mol. Phys.*, 1998, **95**, 71-89.
40. W. Holzer, J. Shirdel, P. Zirak, A. Penzkofer, P. Hegemann, R. Deutzmann and E. Hochmuth, *Chem. Phys.*, 2005, **308**, 69-78.
41. P. J. Hore, E. R. P. Zuiderweg, R. Kaptein and K. Dijkstra, *Chem. Phys. Lett.*, 1981, **83**, 376-383.
42. A. Weller, F. Nolting and H. Staerk, *Chem. Phys. Lett.*, 1983, **96**, 24-27.
43. K. Maeda, T. Miura and T. Arai, *Mol. Phys.*, 2006, **104**, 1779-1788.
44. K. Maeda, A. J. Robinson, K. B. Henbest, E. J. Dell and C. R. Timmel, *J. Am. Chem. Soc.*, 2010, **132**, 1466-1467.
45. R. Leenders, M. Kooijman, A. van Hoek, C. Veeger and A. J. W. G. Visser, *Eur. J. Biochem.*, 1993, **211**, 37-45.
46. T. Kouyama, K. Kinoshita and A. Ikegami, *Eur. J. Biochem.*, 1989, **182**, 517-521.
47. D. R. Kearns, *CRC Critical Reviews in Biochemistry*, 1984, **15**, 237-290.
48. T. A. Early and D. R. Kearns, *Proc. Natl. Acad. Sci. USA*, 1979, **76**, 4165-4169.
49. Y. T. Kao, C. Saxena, T. F. He, L. J. Guo, L. J. Wang, A. Sancar and D. P. Zhong, *J. Am. Chem. Soc.*, 2008, **130**, 13132-13139.